SPECIAL ISSUE PAPER

WILEY

Water budget of tropical volcanic lakes in center-north Cameroon: Reconciling the stable isotope and chloride mass balance

Souleyman Abba[1,2] 🔘 | Bruno Hamelin[1] | Jean-Luc Michelot[3†] | Yannick Garcin[1] | Pierre Deschamps[1]

[1]Aix-Marseille University, CNRS, IRD, INRAE, CEREGE, Aix-en-Provence, France

[2]The University of Ngaoundéré, Faculty of Science, Department of Earth Sciences, Cameroon

[3]GEOPS, Université Paris-Sud, CNRS, Université Paris-Saclay, Orsay, France

Correspondence
Souleyman Abba, CEREGE, Technopole de l'Environnement Arbois Méditerranée, B.P: 13545, Aix-en-Provence, France.
Email: abba@cerege.fr

Funding information
Agence Nationale de la Recherche (TAPIOCA project); French Embassy in Cameroon [Bourse du Gouvernement Français (BGF)]; Institut de Recherche pour le Développement (ARTS Scholarship, LMI DYCOFAC); Labex OT-Med (CALAKE program)

Abstract

The Cameroon volcanic line (CVL) hosts numerous volcanic lakes whose internal processes and hydrological functioning remain poorly documented. A detailed understanding of these hydro-systems is however essential, both for the consideration of these lakes as sentinels of the regional hydro-climatic changes and for the calibration of palaeoenvironmental proxies. Here, we present a hydrological and geochemical investigation of five of these lakes (Mbalang, Tabere, Tizon, Gegouba and Baledjam) around Ngaoundere on the Adamawa Plateau, based on repeated sampling of water profiles and monthly monitoring of rain and lake water samples over two seasonal cycles. We show that each of these throughflow lakes bears a distinct geochemical and isotopic signature, despite quite similar morphometric characteristics and a common climatic regime, due to varying contribution of the watersheds to the water-mass balance and different partitioning between evaporation (E) and outflow (Inflow minus E). We use these differences as a benchmark for a sensitivity analysis of the classical budget equations of conservative tracers. The results demonstrate that to reconcile chloride and stable isotope data with the standard single-box steady state model would require unusual values of the physical parameters of Craig and Gordon's equation such as the $n.\theta$ term that would have to be significantly lower than its usual value ($n.\theta = 0.5$). We also show that the data can be simulated more easily by including the inflow from the watershed while assuming that transpiration exceeds evaporation for this compartment. Using this conceptualization of the throughflow lakes, we were able to constrain the different fluxes. Transpiration from the watershed and evaporation from the lake are on the same order of magnitude, or slightly in favour of

transpiration. While providing evaporation and transpiration rates which are in general in the right order of magnitude, the system of equations remains underdetermined at this stage. Only direct measurements of the isotopic composition of the atmosphere, possible by laser mass spectrometry, would allow to reduce the range of under-determination of this problem.

KEYWORDS
Cameroon, chloride, stable isotopes, volcanic lakes, water budget

1 | INTRODUCTION

Despite the extended progress garnered during the last decades (Lerman et al., 1995), lake studies remain a very active and open field of research. Beyond their important role in the global carbon cycle (Cole et al., 1994), lake systems are understood to be effective sentinels of current climate change (Adrian et al., 2009), since the numerous chemical, physical, hydrological and biological mechanisms that control their internal functioning (e.g., water level, stratification, thermal and mixing dynamics, internal nutrient recycling and productivity) respond to the rapid rates of climate change (e.g., precipitation, runoff, evaporation, temperature; e.g., Butcher et al., 2015; Wang et al., 2018). A recent study by Yao et al. (2023) based on satellite observations reveals a worldwide global decline of water storage in natural lakes over the last three decades. This change in the water balance is mainly attributed to climate warming, increasing evaporative demand and human consumption. However, this study was unable to capture the dynamic of lakes in Africa, with the exception of the massive Eastern African Rift lakes, probably because most of the lakes of Western and Central Africa are too small to apply such global satellite approach. Although these 'small' lakes are far more abundant and that they provide numerous ecosystem services for local populations, including both fisheries and water resources for livestock and domestic use, they remain little studied and their long-term dynamics poorly documented and understood. To date, only a few ground-based studies have provided instrumental records over multiple years of these African tropical lakes to characterize their response to the current climate change (Bader et al., 2011; Bouchez et al., 2016; De Crop & Verschuren, 2019, 2021; Delalande, Bergonzini, & Massault, 2008; Saulnier-Talbot et al., 2014; Wolff et al., 2014).

Quantifying the various components of the water budget is crucial in evaluating the vulnerability of lacustrine systems to climate change and other pressures. However, in remote tropical regions, establishing and maintaining long-term hydrological and meteorological monitoring stations poses significant challenges. To address this issue, isotope and chemical tracers can be useful alternatives to classical hydrological approaches. Stable water isotopes (^{18}O and ^{2}H) have been widely used in hydrological studies of lakes (Awaleh et al., 2015; Bergonzini et al., 2001; Bouchez et al., 2016; Delalande et al., 2005; Delalande-Le Mouëllic et al., 2015; Gat, 1995; Gibson & Edwards, 2002; Gonfiantini, 1986; Kebede et al., 2002; Kebede et al., 2009; Poulin et al., 2019; Vallet-Coulomb et al., 2001). Using the long-standing linear-resistance model of the evaporation process initially proposed by Craig and Gordon (1965), it is possible to assess the isotopic composition of water loss by evaporation and henceforth the stable isotope mass balance. This approach may suffer from many uncertainties, mainly related to a proper adjustment of the input parameters appearing in the Craig and Gordon model (see Delalande, Bergonzini, & Massault, 2008; Kebede et al., 2009 for example). Another widely used technique is the chloride mass balance. Chloride is primarily derived from rainwater, and assuming a conservative behaviour, it can be used as a quantitative tracer of evaporation and evapotranspiration in surface and groundwater (e.g., Branchu & Bergonzini, 2004; Crosbie et al., 2018; Dogramaci et al., 2015; Gurrieri & Furniss, 2004; Saleem & Jeelani, 2017). While both techniques have been frequently used separately, only a handful of them combined the two techniques to better constrain the different terms of the hydrological budget (Calvi et al., 2022; Delalande, Bergonzini, Branchu, et al., 2008; Dinçer et al., 1979; Dogramaci et al., 2015; Kirchner et al., 2010; Nachiappan et al., 2002).

This work is part of a long-term effort to document a cross-continental transect of various lacustrine systems across the climatic gradient in Africa, both for palaeoenvironmental reconstructions (Garcin et al., 2018; Schaaff et al., 2023; Vincens et al., 2010) and hydro-climatic purposes (Adallal et al., 2019; Bouchez et al., 2016; Poulin et al., 2019; Vallet-Coulomb et al., 2001). Although the Cameroon volcanic line (CVL) hosts numerous volcanic lakes, only two of them, Nyos and Monoun, have been extensively studied following the catastrophic releases of CO_2 in 1984 and 1986 (Kling et al., 1987; Sigurdsson et al., 1987; Tanyileke et al., 2019). Other lakes such as those on the Adamawa Plateau in the center-north region of Cameroon remain poorly documented. Sediment cores were collected previously from Mbalang and Tizon (Ngos & Giresse, 2012; Nguetsop et al., 2011; Vincens et al., 2010). Tabere, Gegouba, Baledjam and Tizon were visited in the course of general surveys of the CVL lakes for stable isotopes (Issa, Aka Tongwa, et al., 2014) and for CO_2 emission assessment (Issa, Ohba, et al., 2014). However, the present paper reports the first systematic comparative study of this series of lakes by collecting an initial database relating to the hydrological, geochemical and isotopic functioning of these tropical hydro-systems.

In this study, we propose to couple the isotopic and chloride mass balance techniques to assess the hydrological budget of five crater lakes (Mbalang, Tabere, Tizon, Gegouba and Baledjam) located in the northern part of the CVL, in the vicinity of the town of Ngaoundere
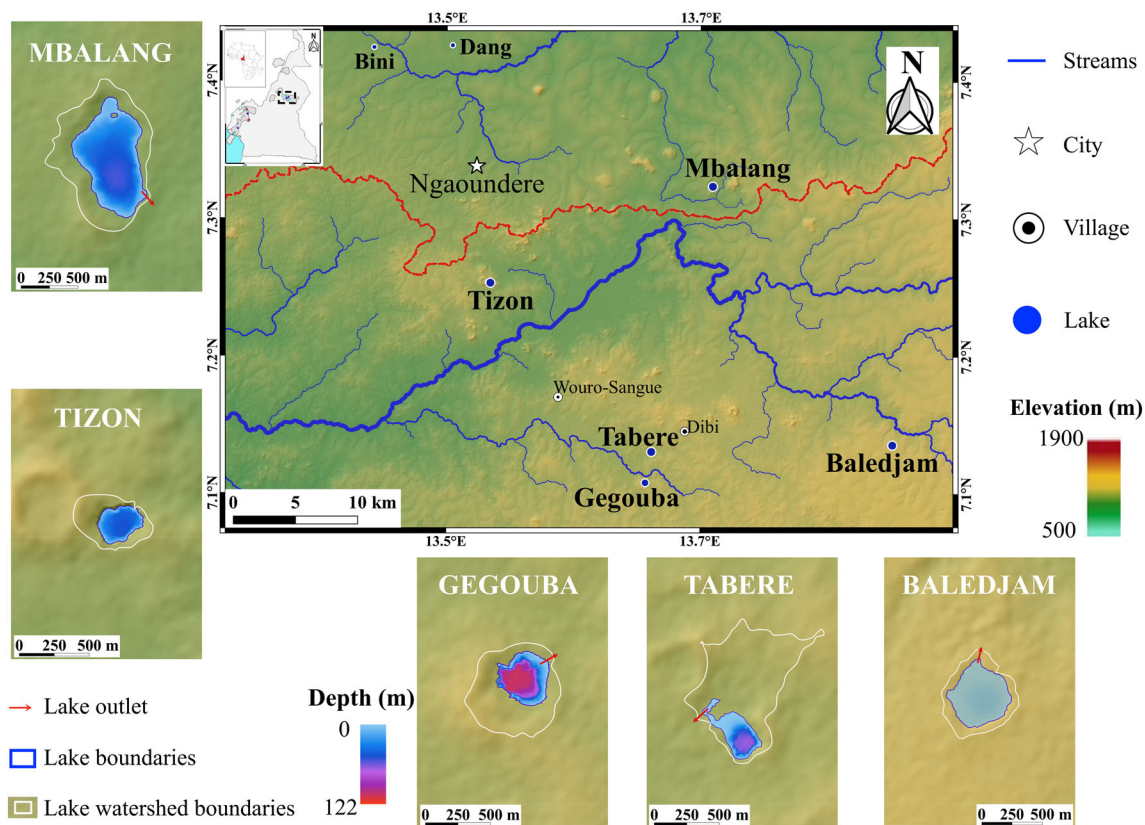
FIGURE 1 Topographic map of the Adamawa plateau around Ngaoundere and location of the five investigated maar lakes. Inserts show the dimension and bathymetry of the five lakes and the topography of their watersheds. Small red arrows indicate the position of temporary outflows. The dashed red line bounds northern-vina and southern-vina watersheds.

(Figure 1). Because this series of lakes are located within a restricted geographic area under similar climatic conditions, they represent an ideal setting to test and cross-check the isotope and chloride mass balance approaches and to investigate specific questions regarding these two independent methods that were rarely addressed in the literature. In particular, we aim to address the following questions:

1. Do water stable isotopes and chloride budgets provide the same hydrological constraints on the lake evaporation flux? If not, how can the isotope and chloride mass balances be reconciled?
2. Does the combination of these two approaches allow a better assessment of the different terms of the water budget?

The data we have collected will serve as a background for continuous monitoring of these lakes in their role as possible sentinels of regional hydro-climatic changes. Specifically, we investigated the stratification of these lakes by intermittent water-column profiling; we carried out, on a monthly basis, isotopic and chemical monitoring of their water columns as well as the rainfall. This complete database allows us to use the slight variations in stable isotopes and chemical composition between these five lakes as a benchmark enabling to evaluate the sensitivity of the hydrological budget equations to the choice of parameters involved in the Craig and Gordon model. In particular, we discuss the constraints derived from coupling stable isotopes and chloride budgets,

a condition seldom considered in previous studies (Dinçer et al., 1979; Dogramaci et al., 2015; Gat, 1995). In addition, the relatively small size and well delineated geomorphology of the studied systems allows us to examine thoroughly the influence of the watershed inflow on the lake water budget, a parameter which is generally very difficult to evaluate in larger basins (Adallal et al., 2019; Masse-Dufresne et al., 2021).

2 | STUDY SITE

2.1 | Climate

The region of the Adamawa Volcanic Plateau is characterized by an altitudinal tropical climate marking the transition between Equatorial and Sahelian climates, with two contrasted seasons: rainy from April to October, and dry from November to March (Suchel, 1988). The (2000–2017) record of meteorological data used herein was communicated by the Ngaoundere airport weather station (Figure SI-1). Average annual precipitation is 1464 mm (inter-annual range from 1166 to 1817). The seasonal cycle of average monthly temperatures shows a minimum of 19.5°C from December to January at the peak of the dry season, and a maximum of 24.5°C in March. Evaporation pan data also show a pronounced seasonal cycle, with between 98 and 244 mm per month, and an annual amount average of 1800 mm.

TABLE 1 Morphometric features of Adamawa lakes [Residence times are calculated as ratio of lake volume (m^3) over rainfall (m^3/y)].

Lake	Surface area (ha)	Volume ($*10^6$ m^3)	Maximum depth (m)	Average depth (m)	Watershed surface area (ha)	Residence time (years)
Mbalang	42	12	55	29	78	20
Tabere	8	2	70	24	57	18
Tizon	6	2	52	30	16	24
Gegouba	12	7	122	58	40	42
Baledjam	19	1	13	7	31	4

Relative humidity is strongly variable on a diurnal cycle. However, it also follows a seasonal cycle, with 2000–2017 average monthly minima increasing from 20% in February to 66% in August, and monthly maxima from 69% to 98% (Figure SI-1). Mean annual values of $h = 63\%$ and $t = 21.6°C$ are then calculated by weighting monthly values by the corresponding evaporation flux, resulting in the key parameters used in the evaporation model discussed below.

2.2 | Geomorphology and hydrology

As is the case for most other lakes along the CVL, the Adamawa lakes are hosted in maars formed in recent trachytic or basaltic series overlain by pyroclastic materials (Kling, 1988). The watersheds are mostly covered by ferralitic soils. Rock outcrops represent less than 1% of the surface at Mbalang, Tabere, Tizon and Baledjam watersheds, and about 5% at Gegouba (Wirrmann, 1994). The basement is composed of granites on one hand and volcanic formations on the other. Granites appear as 50 km wide NW-SE strips bordered by Precambrian metamorphic rocks. The volcanic formations belong to the three series described by Gèze (1943) along the CVL: lower basaltic and andesitic black series from the Upper Cretaceous to Upper Eocene, middle white series (Late Neogene) corresponding to trachytic and phonolitic lavas, and upper mainly basaltic Quaternary black series.

In terms of vegetation, the watersheds are covered by savanna with dominant *Hyparrhenia fillipendula*, *Daniella Oliveri* and *Lophira lanceolata* (Rippstein, 1986). Some variations are observed between the lakes, such as clusters of trees (*Croton macrostachys*, *Khaya senegalensis*) at Mbalang, while Tizon has a herbaceous cover with copses of wide isolated shrubs (Ngos & Giresse, 2012). The lakes are in general quite isolated, with relatively little human activity. The agricultural imprint is very limited, with some slash-and-burn farming and cattle herding at Mbalang, and crop growing at Tabere and Baledjam.

The main morphological characteristics of the lakes are summarized in Table 1. Their altitudes range between 1150 and 1258 m, and surfaces from 0.07 to 0.42 km^2. Baledjam is the only shallow lake (13 m maximum deep), compared with the other four that are quite deep (48–104 m maximum depths). Tabere is the only lake with a wide watershed, almost sevenflod larger than the lake itself, while only twofold to threefold for the other four. The watersheds are steep-sided and funnel-shaped, with rims culminating from 50 to 70 m above the lake level except at Baledjam, which is in a more open

site. Tizon is the only fully endorheic lake. In the other cases, temporary overflow thresholds, active only during the rainy season, can be observed (Figure 1). For Mbalang Lake, the water level reaches the overflow threshold only at the very end of the rainy season. In current climate conditions, the amplitude of variation between low-stand and overflow is between 0.65 and 0.85 m, that is 2%–3% of the lake volume.

The groundwater configuration beneath the lakes is essentially unknown. At Mbalang, the closest well is located 300 m away from the lake on the outer slope of the maar, with an observed water table depth estimated at roughly 15 m below the lake level.

The range of water residence time is from 4 to 45 years (Table 1). These first order estimates based on the lake volume-rainfall ratio may be reduced proportionately to the watershed-lake surface ratio, depending on the fraction of runoff from the watershed to the lake.

3 | MATERIALS AND METHODS

3.1 | Sampling

Depth profiles were sampled on the five lakes during two field campaigns in mid-March 2019 and early-March 2020. Three shallow lakes (Bini, Dang and IRAD) were also sampled for comparison (Figure 1). In addition, Mbalang, Tabere and Tizon were visited 14 times over the seasonal cycle from April 2020 to October 2021. Water samples were collected at the deepest point of the lakes using a 3.2 L WILDCO water sampler (Vertical Alpha bottle model). Prior to sampling, the structure of the conductivity-temperature-depth profile was first measured by a Hydrolab HL4 in situ profiler (OTT Hydromet), as were pH, Eh and dissolved O_2.

Surface water temperature, conductivity and lake level were also monitored continuously at Mbalang by means of a pair of Solinst probes installed within the water column (Levelogger LTC) and above the surface on the shore of an island (Barologger) during the 2 years of our study.

Eighteen rainwater samples were also collected on a monthly basis at our Mbalang-Djalingo weather station (3 km from Mbalang lake) during the wet seasons of 2020 and 2021. We used a PALMEX RS2 rain sampler, designed to minimize water evaporation from the 10 L collecting bottle. At each visit, samples were taken in two 30 mL LDPE bottles for the analysis of chloride and major cations contents, and in 30 mL airtight amber glass bottles for stable isotopes analysis. The remainder of the sample was kept in anticipation of ^{36}Cl analyses,

the results of which will be reported separately. Annual means and seasonal trends of the meteorological data obtained at this local station were coherent with those from Ngaoundere Airport.

3.2 | Experimental techniques

For each water sample, whether from rain or from the lakes, the basic physico-chemical parameters [temperature, pH, Electrical Conductivity (EC), Dissolved Oxygen and Redox Potential] were measured immediately upon recovery in the field with a HACH multiparameter probe. Alkalinity was first measured by H_2SO_4 titration with bromocresol green indicator at the hotel in the evening, and was later measured again more accurately with a HACH automatic titrator (TITRALAB AT1000) upon return to the laboratory.

The concentrations in major ions were determined by ion chromatography using a DIONEX AQUION. All samples were filtered through 0.45 μm filters before measurement. The precision and accuracy of our results were assessed through repeated measurements of certified standards in parallel to each series of samples (Table SI-1), with particular attention paid to the most diluted rain samples. As an additional test of the reliability of our results, we also replicated a series of chloride analyses by isotope dilution with a spike solution enriched in ^{35}Cl, measured on the ASTER AMS at CEREGE along with the ^{36}Cl determination, as described by Bouchez et al. (2015). The results of the two independent techniques are in agreement within 10% on average throughout the range of concentrations, with a maximum difference of 15% for the lakes, and 23% for the low concentrations in rain data.

The isotopic compositions of oxygen and hydrogen were analysed at GEOPS (Paris Orsay) on a laser spectrometer LGR (Los Gatos Research) OA-ICOS TLWIA-EP-45. Each sample was injected (600 μL) seven times, with only the three last injections taken into account to avoid any memory effect. Three working standards, calibrated versus V-SMOW2 and SLAP2, were used: MAZA ($\delta^2H = 1.54‰ ± 1$; $\delta^{18}O = −1.13‰ ± 0.03$), DIDO2 ($\delta^2H = −49.33‰ ± 0.8$; $\delta^{18}O = −7.22‰ ± 0.06$), NAN ($\delta^2H = −65.49‰ ± 0.8$; $\delta^{18}O = −9.43‰ ± 0.03$). The final result was obtained from three replicates to check that standard deviation was lower than 0.6‰ for ^2H and 0.2‰ for ^{18}O. Precision was also validated by long-term repetition of a control sample in each series. Results are reported in delta notation, ‰ versus V-SMOW.

The isotopic composition of strontium was measured on a Neptune+ MC-ICPMS at CEREGE, using a standard chemical procedure (Yeghicheyan et al., 2021). The mean result obtained on NBS 987 is $^{87}Sr/^{86}Sr = 0.71025 ± 0.00002$, (2sd, $n = 20$), and that obtained on the VWR standard is $^{87}Sr/^{86}Sr = 0.70755 ± 0.00002$ (2sd; $n = 15$).

3.3 | Isotopic and chloride budget

As an initial step, we first recall the equations describing the simplest case of a one-box model, assuming steady state and homogeneity, to simulate a lake which receives an input flux of water (I) from precipitation only, and loses water through both evaporation (E) and outflow ($I − E$) carried by surface streams and subsurface seepage. Indeed, the lakes studied herein receive no water from upstream rivers. However, the possible contribution of water flowing into the lake from its watershed will be taken in consideration in a second step, below.

In this first simple case, the water budget is expressed classically using either the mass balance of chloride (Equation 1) or that of stable isotopes (Equation 2):

$$\frac{E}{I} = 1 - \frac{C_I}{C_L} \tag{1}$$

$$\frac{E}{I} = \frac{\delta_I - \delta_L}{\delta_E - \delta_L} \tag{2}$$

C_I and C_L are chloride concentrations, δ_I and δ_L, isotopic compositions of oxygen or hydrogen of the inflow and lake water, respectively. In this simple model, since rain is the only water supply to the lake, C_I is equal to C_P and δ_I to δ_P. C_P and δ_P are average values of the rain data, weighted by the rainfall amount.

The isotopic composition δ_E of oxygen or hydrogen of the evaporation flux is calculated classically with Craig and Gordon's (1965) equation, as written for instance in Gibson and Edwards (2002) and Gat (2010):

$$\delta_E = \frac{\left[\left(1 - \frac{\varepsilon^*}{1000}\right) \cdot \delta_L - h.\delta_A - (\varepsilon^* + \varepsilon_k)\right]}{\left(1 - h + \frac{\varepsilon_k}{1000}\right)} \tag{3}$$

The difference between δ_L and δ_E thus depends on the relative humidity (h), and on the isotopic composition of atmospheric vapour (δ_A). ε^* is the corresponding equilibrium isotopic separation ($\varepsilon^* = (1 − \alpha^*).10^3$) where the term α^* is the liquid to vapour isotope fractionation factor (<1) for which we use the expression given by Horita and Wesolowski (1994) (Supporting Information).

As in Gat (2010), we formulate the kinetic isotopic separation (ε_K), as:

$$\varepsilon_k = C_k.n.\theta.(1 - h) \tag{4}$$

C_k is the ratio of molecular diffusivities of the heavy over light isotopologue molecule, using the values determined by Merlivat (1978) ($C_k = 28.5‰$ and 25.1‰ for ^{18}O et ^2H, respectively). The term (n) is the exponent of the relationship between diffusivity and resistance to transport and depends on the state of turbulence of the atmosphere over the lake (n = 1/2 for fully turbulent conditions, and n = 1 for stagnant air). θ is the ratio of resistance to transport in the diffusive layer over the total resistance in diffusive and convective layers. It is related to the intensity of recycling of the vapour evaporated from the lake into the local atmosphere ($\theta = 1$ for a small water body with no significant recycling; Gat, 2010).

In previous studies, a value of 0.5 has quite often been assumed for the term $n.\theta$ as being most representative of open water natural

conditions (e.g., Araguás-Araguás et al., 2000; Gibson et al., 2016; Gibson & Edwards, 2002; Gonfiantini, 1986; Jasechko et al., 2013). However, it has also been shown that lower values of θ must be considered when the atmospheric moisture is strongly influenced by vapour recycled from the open water surface. This was first demonstrated in the case of very large water surfaces such as the Great Lakes (Gat et al., 1994) and the Eastern Mediterranean Sea (Gat et al., 1996) (θ = 0.88 and 0.5, respectively). However, this has also been shown by Kebede et al. (2009) for much smaller lakes in Ethiopia, some of which are comparable in size and settings to those of the present study. We will therefore consider n.θ as a floating parameter in our discussion below, in order to test the sensitivity of the results of our model to this factor.

Provided that the parameters remain constant, δ_E, δ_I and δ_L remain aligned along a single 'local evaporation line' (LEL) in the isotope plot (Gat, 1995, 2010; Gibson et al., 2016). The slope S_{LEL} of the LEL links the δ_A values of oxygen and hydrogen with n.θ when h and $t°C$ are known:

$$S_{LEL} = \frac{[h(\delta_A - \delta_I) + \varepsilon^* + \varepsilon_k]_{2_H}}{[h(\delta_A - \delta_I) + \varepsilon^* + \varepsilon_k]_{18_O}} \quad (5)$$

For given climatic conditions ($t°C$, h), one can then seek appropriate values of ($\delta_A^{18}O$, $\delta_A^{2}H$, n.θ) required to fit the observed slope of the LEL. In order to reduce the number of unknowns, we make the simplifying assumption in all the following calculations that the isotopic composition of atmospheric vapour lies on the GMWL. Under this condition, $\delta_A^{18}O$ is thus linked directly to n.θ. The three Equations (1), (2) and (5) with three unknowns (E/I, n.θ and δ_A) thus have a single solution. The E/I ratio is uniquely determined, and the chloride and isotopic budgets are coherent.

The assumption made concerning the atmospheric vapour composition is clearly a first order hypothesis adopted for practical purposes, ignoring the effect of recycled water vapour. Implications of this assumption will be discussed below.

A second step of our approach aims at testing the influence of the inflow from the watershed on the water budget of the lake. A schematic of the model modified to take this contribution into account is shown in Figure SI-2. In order to maximize the influence of the input from the watershed on the comparison between the isotopic and chloride budgets, we consider here the simplified case where transpiration from the vegetation (flux T) largely dominates evapotranspiration on the watershed ($E_{watershed} = 0$). Indeed, it is well accepted that transpiration does not fractionate stable isotopes (Dinçer et al., 1979; Yakir & Wang, 1996), while it does leave residual water enriched in chloride. The rainfall flux on the watershed is thus split between transpiration (T), infiltration through the unsaturated zone over the watershed (INF) that escapes from the lake system, and input to the lake either as surface runoff or subsurface flow (i.e., P − INF − T; Figure SI-2). Within this framework, the water input to the lake from the watershed retains the same isotopic composition as the rain, that is, $\delta_I = \delta_P$, while its concentration in chloride (C_{wsh}) is increased due to the transpiration.

In this scheme, the budget equations become (see Supporting Information for explicit derivation):

$$C_P \cdot \left[1 - \frac{INF}{P} \cdot \frac{1}{\left(1 - \frac{T}{I}\right)} \cdot \frac{S_{wsh}}{S_{tot}}\right] = C_L \cdot \left[1 - \frac{S_{wsh}}{S_{tot}} \cdot \frac{(T + INF)}{I} - \frac{S_L}{S_{tot}} \cdot \frac{E}{I}\right] \quad (6)$$

$$\begin{aligned} \delta_P \cdot \left[1 - \frac{(T + INF)}{I} \cdot \frac{S_{wsh}}{S_{tot}}\right] - \chi \cdot \frac{E}{I} \cdot \frac{S_L}{S_{tot}} \\ = \delta_L \cdot \left[1 - \frac{(T + INF)}{I} \cdot \frac{S_{wsh}}{S_{tot}} + \frac{E}{I} \cdot \frac{S_L}{S_{tot}} \cdot (\varphi - 1)\right] \\ \text{with } \chi = \frac{-(h\delta_A + \varepsilon^* + \varepsilon_k)}{1 - h} \text{ and } \varphi = \frac{1}{1 - h} \end{aligned} \quad (7)$$

in which S_L, S_{wsh} and S_{tot} are the surfaces of the lake alone, the watershed (not including the lake), and the total, respectively.

Equation (7) may use $\delta_A^{18}O$ or $\delta_A^{2}H$ indifferently, since the isotopic compositions of L, P and E are aligned along the LEL in the isotope plot, and are thus linearly related. All calculations below are carried out with $\delta_A^{18}O$.

The set of three Equations (5), (6) and (7) with four unknowns (E/P, T/P, n.θ, δ_A) is undetermined. For a given value of n.θ, a unique set of values of E/P and T/P can thus be obtained.

In each simulation, we first determine a set of (δ_A, n.θ) compatible with the observed slope of the LEL (Equation (5)). Examples of solutions are illustrated in Figure SI-3.

Then, for each selected pair (δ_A, n.θ), we adjust the E/P and T/P values required to fit the target lake composition of [Cl⁻] and $\delta^{18}O$. Specific trajectories of δ_L and C_p can be illustrated in the $\delta^{18}O$ versus [Cl⁻] diagram by varying E/P and T/P separately, according to Equations (6) and (7). The influence of the additional variable INF/P can then be evaluated by comparison with one selected solution in which INF/P = 0.

4 | RESULTS

4.1 | Stratification

The temperature profiles measured during the two exhaustive campaigns in March and during regular visits between April and October are shown in Figure 2a. The thermocline can be seen to deepen gradually from March to October, with a maximum depth of the inflexion point of the thermal gradient at 10–14 m in each lake, except in the shallower Lake Baledjam where the gradient is smoother.

The range of seasonal surface temperature variation recorded by the probe installed permanently at Mbalang is from 20 to 26°C, with a steep decrease starting in October and a pronounced minimum at the height of the dry season in January (Figure 2b). By contrast, the temperature profiles from one visit to the next are strictly reproducible below the thermocline, and show only slight variation with depth in general: either unchanged below 10 m as at Gegouba, or with a smooth decrease of about 0.8°C from 10 to 35 m at Mbalang. The deep temperatures vary slightly between the lakes, from 20.1°C at
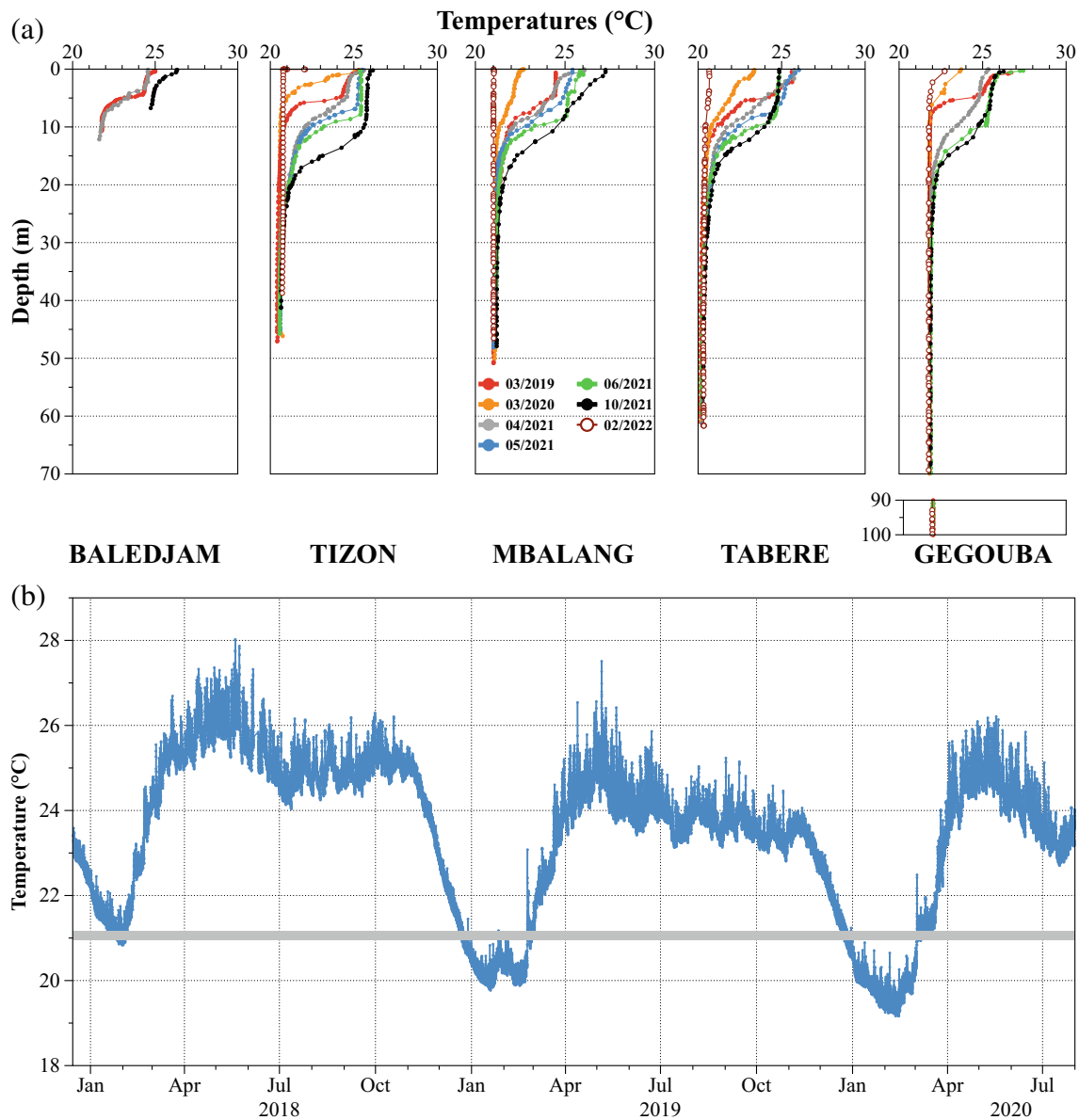
FIGURE 2 Temperature data. (a) Depth profiles of temperature (°C); (b) temperature record of the surface water probe at Mbalang. The horizontal line indicates the temperature below the seasonal thermocline.

Tabere to 21.9°C at Gegouba, and are broadly correlated with the volume/surface ratio.

Finally, the comparison between the permanent probe record and the depth profile at Mbalang shows that surface water temperature approaches temperature at depth during the winter minimum. This suggests a monomictic behaviour of this lake, in agreement with the list of criteria proposed by De Crop and Verschuren (2019) and based on observation of a series of Ugandan lakes. This allows us to infer the same tendency for the other lakes, except that more frequent mixing probably occurs at the shallower Lake Baledjam.

4.2 | Chemical composition

All chemical and isotopic data are listed in Tables 2 and 3.

All the lakes are characterized by low electrical conductivities, ranging from 115 to 290 μS/cm. This is typical of 'throughflow lakes' (Gat, 2010; Gibson et al., 2016) from which the dissolved load is continuously exported out of the lake by its outflow and by seepage towards groundwater, allowing the regulation of the lake's chemistry. In all the cases we studied, conductivity profiles increase with depth, from 15% to 38% for Mbalang, Gegouba, Tizon and Baledjam, but by a factor of more than 2 in the case of Tabere. The profiles are clearly distinct from each other, making it possible to rank Baledjam, Tabere, Mbalang, Gegouba and Tizon on an increasing scale of salt content in surface water (Figure SI-4). These differences are reproducible from one visit to the next, although small but significant variations can be observed in both subsurface and deep waters during the seasonal cycle.

The results for the carbonate system are illustrated in Figure SI-4. Alkalinity values range from 0.95 meq/L (Baledjam) to 2.5 meq/L

TABLE 2 Physico-chemical and chemical compositions of Adamawa lakes.

Samples	Depth	pH	EC	Cl⁻	NO₃⁻	F⁻	HCO₃⁻	Na⁺	K⁺	Mg²⁺	Ca²⁺	NH₄⁺	Sr²⁺	Ionic balance	$\delta^{18}O$	$\delta^{2}H$	$^{87}Sr/^{86}Sr$
	m		µS/cm	µeq/l										%	(‰)		
Mbalang 2019	1	7.9	173	17.5	3.4	9.1	1609	252	104	783	589	<dL	2.8	2.7	4.95	24.47	0.704
	3	7.9	173	20.2	3.7	9.2	1624	252	103	786	589	<dL	2.9	2.2	4.84	24.54	0.704
	6	7.9	173	17.7	3.4	9.0	1600	252	103	783	587	<dL	<dL	2.8	4.80	24.31	0.704
	9	7.6	169	17.2	4.2	8.9	1580	246	100	764	574	<dL	<dL	2.2	4.74	24.39	0.704
	15	7.0	169	17.3	11.2	8.7	1566	246	101	764	576	<dL	2.8	2.6	4.68	23.64	0.704
	20	6.7	169	16.9	12.0	8.9	1539	244	100	762	570	<dL	<dL	3.0	4.86	22.99	0.704
	25	6.7	179	17.1	2.1	9.0	1555	245	100	763	603	<dL	<dL	3.9	4.69	23.65	0.704
	30	6.3	188	17.0	<dL	8.9	1534	246	100	767	597	73	<dL	6.7	4.68	22.67	0.704
	40	6.3	205	18.2	<dL	8.9	1489	248	101	777	600	122	<dL	9.9	4.64	23.08	0.704
	50	6.2	212	17.1	<dL	8.8	1486	248	101	774	601	125	2.9	10.1	4.99	23.58	0.704
Mbalang 2020	2	7.7	166	17.8	<dL	7.5	1513	246	103	763	606	<dL	2.6	5.6	4.71	21.33	-
	5	7.7	165	16.6	<dL	7.6	1564	246	103	770	615	<dL	2.8	4.5	4.69	22.28	-
	10	7.0	165	17.2	<dL	7.7	1630	243	101	761	606	<dL	2.7	1.7	4.51	21.93	-
	20	7.0	165	16.7	<dL	7.6	1601	243	101	757	593	<dL	2.7	2.2	4.48	21.02	-
	35	7.0	168	16.7	<dL	8.1	1683	244	101	762	605	<dL	2.8	0.2	4.44	21.16	-
	50	7.1	170	16.7	<dL	7.6	1628	243	102	765	610	<dL	2.9	2.1	4.52	21.59	-
Mbalang	Mean	7.1	176	17.4	5.7	8.5	1575	246	102	769	595	107	2.8	-	4.70	22.91	0.704
Tabere 2019	2	7.8	148	18.7	7.6	7.1	1363	241	55	684	485	<dL	2.9	2.5	2.31	10.05	0.706
	30	6.9	168	15.9	<dL	6.4	1310	239	54	680	503	118	<dL	9.1	1.63	7.12	0.706
	55	7.3	269	17.9	<dL	7.4	1540	265	59	719	564	322	<dL	10.4	1.50	6.72	0.706
Tabere 2020	2	7.4	137	15.1	7.5	5.4	1400	231	52	660	487	<dL	2.6	0.2	1.13	3.92	-
	5	7.3	137	15.7	7.6	6.2	1445	230	52	663	493	<dL	2.9	−1.2	1.20	3.43	-
	10	6.9	137	15.7	5.1	5.8	1381	226	51	652	489	<dL	2.6	0.5	0.76	1.89	-
	30	6.8	152	17.3	<dL	6.3	1408	233	53	664	509	89	3.0	4.0	1.10	3.93	-
	50	6.8	246	16.2	<dL	7.2	1924	266	61	729	590	345	3.8	1.2	-	-	-
	55	-	-	16.5	<dL	12.1	<<dL	273	62	740	602	401	4.0	-	1.44	6.57	-
Tabere	Mean	7.2	174	16.6	7.0	7.1	1471	245	55	688	525	255	3.1	-	1.38	5.45	0.706
Tizon 2019	2	8.1	282	33.5	12.6	24.1	2563	621	218	955	1044	<dL	6.2	3.9	5.46	25.54	0.705
	10	7.1	272	28.8	32.5	23.4	2525	602	212	927	1008	129	<dL	2.6	5.18	23.96	0.705
	30	7.1	293	28.4	<dL	23.6	2444	604	213	929	1020	<dL	<dL	7.4	5.09	24.00	0.705
Tizon 2020	2	8.3	-	30.6	5.6	23.8	2560	610	219	1028	1026	<dL	5.5	8.4	5.06	22.00	-
	5	7.3	264	28.9	4.0	23.3	2584	602	216	1011	988	33	5.5	9.1	4.81	20.55	-

TABLE 2 (Continued)

| Samples	Depth	pH	EC	Cl⁻	NO₃⁻	F⁻	HCO₃⁻	Na⁺	K⁺	Mg²⁺	Ca²⁺	NH₄⁺	Sr²⁺	Ionic balance	δ¹⁸O	δ²H	⁸⁷Sr/⁸⁶Sr
	m		µS/cm	µeq/l										%	(‰)		
	10	7.2	267	28.6	<dL	23.4	2622	600	215	1011	1011	50	4.7	10.1	4.62	20.73	-
	30	7.3	267	28.6	<dL	23.3	2640	598	214	1006	1009	68	5.3	11.5	4.67	20.74	-
	45	7.0	289	28.6	<dL	23.5	2649	604	216	1021	1030	156	5.5	9.1	4.93	21.42	-
Tizon	Mean	7.4	276	29.5	13.7	23.5	2573	605	215	986	1017	87	5.5	-	4.98	22.37	0.705
Gegouba 2019	2	7.5	199	10.7	<dL	8.3	1866	261	75	856	724	65	3.7	2.6	3.36	14.36	0.705
	7	6.9	197	9.2	<dL	7.8	1877	256	73	839	716	89	<dL	2.0	2.83	13.10	0.705
	20	7.0	202	10.5	<dL	8.0	1844	255	73	840	714	93	<dL	2.9	2.80	12.28	0.705
	50	7.0	203	9.1	<dL	8.1	1826	255	73	838	711	93	<dL	3.3	2.85	12.19	0.705
Gegouba 2020	2	7.5	189	9.2	<dL	7.1	1798	263	76	951	785	68	3.4	4.9	2.86	11.60	-
	5	7.2	189	9.3	<dL	7.6	1743	261	76	939	763	71	3.7	3.8	2.83	11.86	-
	10	6.9	193	9.5	<dL	7.2	1698	257	74	927	759	81	3.7	3.8			-
	20	6.9	193	9.4	<dL	7.1	1647	257	75	925	754	81	3.6	3.7	2.66	11.38	-
	50	6.9	193	9.2	<dL	7.2	1730	258	75	925	753	81	3.4	5.8	2.61	10.70	-
Gegouba	Mean	7.1	195	9.6	<dL	7.6	1781	258	74	893	742	80	3.6	-	2.85	12.18	0.705
Baledjam 2019	2	7.9	114	14.2	<dL	5.8	1038	81	55	570	407	0	1.9	2.6	4.14	20.45	0.705
	10	6.5	119	12.1	<dL	5.8	999	79	54	561	408	29	<dL	5.3	3.73	18.17	0.705
Baledjam	Mean	7.2	116	13.1	<dL	5.8	1019	80	54	565	407	29	1.9	-	3.94	19.31	0.705
Dang		6.0	56	68.4	<dL	<dL	419	195	<dL	73	235	<dL	2.1	1.8	6.91	31.62	0.708
Bini		6.0	18	3.0	<dL	<dL	140	42	<dL	44	64	<dL	<dL	2.5	0.88	4.17	0.707
IRAD		6.4	43	16.0	<dL	6.0	326	59	54	173	119	<dL	<dL	7.5	8.30	40.30	0.709

Note: For each lake, the first and second dataset represents data collected in 2019 and 2020, respectively. Arithmetic mean values are calculated over the 2 years of collection for lake samples. EC: Electrical Conductivity, (<dL) under detection limit, (-): not measured.

TABLE 3 Physico-chemical and chemical compositions of rain samples at Mbalang.

Samples	Sampling date	Days	Rainfall amount	pH	EC	Cl⁻	NO₃⁻	F⁻	Na⁺	K⁺	Mg²⁺	Ca²⁺	NH₄⁺	δ¹⁸O	δ²H
			mm		µS/cm	µeq/l								(‰)	
2020															
#1	04/04/2020	13	74.65	6.3	41	9.4	37.4	0.5	7.0	14.5	20.4	93.0	72.2	−0.87	4.80
#2	01/05/2020	27	79.47	5.6	30	9.4	17.6	0.3	9.1	15.4	12.2	49.2	179.4	0.60	15.39
#3	31/05/2020	30	252.85	5.3	8	3.0	14.3	0.1	2.4	2.2	3.4	26.3	16.3	−3.09	−11.11
#4	30/06/2020	30	120.41	6.3	8	3.3	10.9	0.2	2.2	2.0	3.5	27.7	0.7	−4.11	−19.40
#5	15/07/2020	15	125.22	4.8	21	2.1	8.8	0.1	0.8	1.9	1.2	9.8	1.9	−4.50	−24.22
#6	15/08/2020	31	122.81	5.7	4	2.8	6.7	0.1	1.3	2.3	1.4	10.3	4.8	−7.32	−47.16
#7	15/09/2020	31	161.34	-	-	1.8	4.0	<dL	0.6	1.1	0.8	11.1	1.6	−9.12	−63.67
#8	16/11/2020	62	216.73	-	-	4.7	<dL	<dL	2.0	2.0	2.2	28.2	3.5	−5.23	−29.60
2021															
#1	03/05/2021	15	112.80	5.7	21	5.1	15.5	0.3	3.4	2.9	5.6	67.8	28.2	0.34	18.10
#2	27/05/2021	24	229.60	5.6	16	2.9	6.0	0.3	1.3	1.1	2.7	42.9	66.1	−5.08	−26.84
#3	16/06/2021	20	109.80	7.2	15	6.1	10.0	0.3	3.0	1.9	4.5	66.6	2.5	0.61	19.63
#4	01/07/2021	15	87.20	7.0	28	6.1	16.8	0.4	2.8	2.0	6.2	95.1	2.8	−2.18	−1.24
#5	16/07/2021	15	254.20	6.2	21	4.4	10.4	<dL	2.0	2.2	4.4	38.3	30.2	−4.63	−23.32
#6	01/08/2021	16	82.20	7.7	13	6.1	25.2	<dL	2.8	5.5	4.0	40.0	19.6	−2.89	−9.00
#7	17/08/2021	16	162.00	5.2	17	2.4	11.1	<dL	0.9	1.8	1.4	20.8	<dL	−6.07	−36.56
#8	01/09/2021	15	155.20	5.8	12	3.9	<dL	<dL	2.0	1.2	3.0	46.8	1.4	−6.67	−41.74
#9	16/09/2021	15	108.00	7.0	13	3.6	10.4	0.3	2.0	1.4	4.3	52.9	0.4	−5.98	−35.42
#10	01/10/2021	15	170.00	6.2	6	2.8	3.0	<dL	1.6	0.9	2.6	31.7	<dL	−5.61	−33.43
Weighted mean rainfall 2020–2021				-	-	4.0	11.3	0.2	2.2	2.7	3.8	37.8	22.0	−4.44	−22.76

Note: The average 2020–2021 value of rain samples is weighted by rainfall amount. EC: Electrical Conductivity, Days refer to the time elapsed before sampling, (<dL) under detection limit, (-): not measured.

FIGURE 3 Depth profiles of δ¹⁸O and Cl⁻ concentrations. The lower panel shows the results of samples collected in March 2019 and 2020. The upper panel shows the seasonal variability in surface samples collected regularly from April 2020 to October 2021.
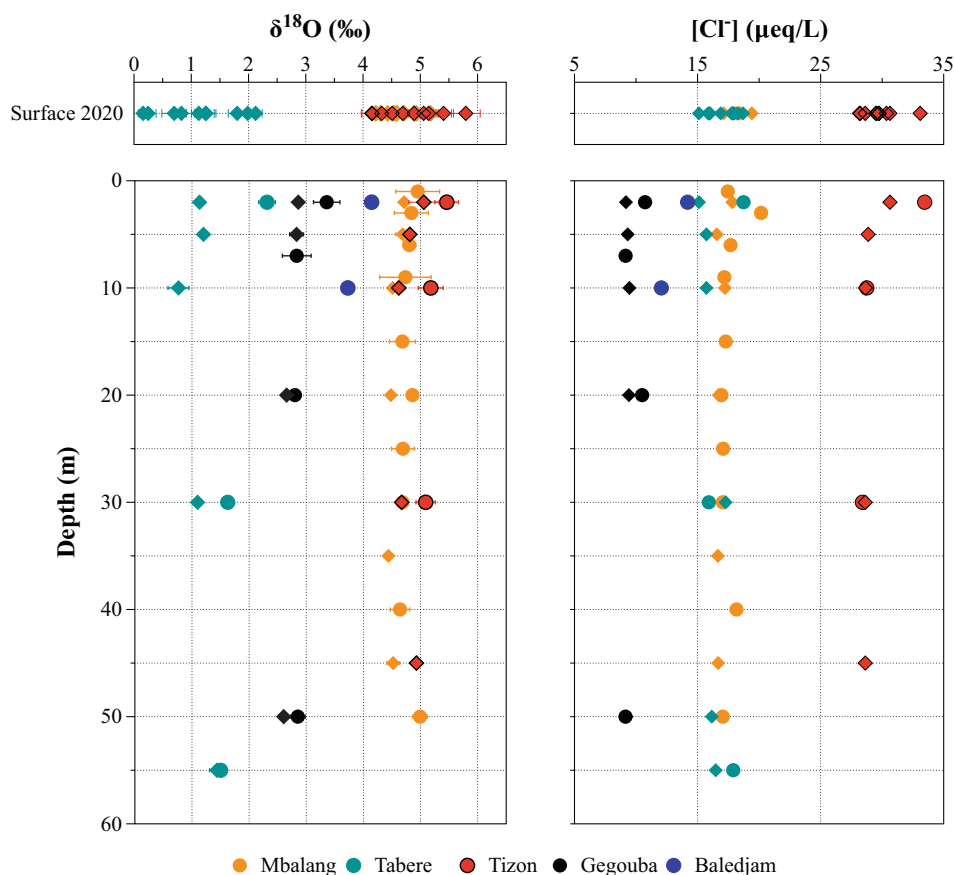
(Tizon) and are well correlated with EC (Figure SI-5), which is coherent with the observation that HCO_3^- represents at least 97% of total anions (Table 2). The pH profiles are strongly stratified, with a sharp decrease of 1–1.5 pH unit between the upper levels and the deep waters, clearly associated with the thermocline and the decrease in oxygen content (Figure SI-4). The pH values are constant with depth and are very similar between the different lakes in the deep waters (6.9–7.3). Seasonal variations are observed in surface water in all the lakes, with pH values increasing to 8.5–8.8 during the wet season, with the exception of slightly more acidic conditions at Tabere Lake (8.0).

In all the lakes, the depth profiles of pH and dissolved O_2 are strikingly similar, with the water becoming anoxic just below the thermocline (Figure SI-4).

These features are clear indicators of the biological control on the carbon cycle of these lakes. The CO_2 partial pressure (p_{CO2}) is close to equilibrium with the atmosphere at the surface and enhanced at depth, due to the downward transfer and degradation of the organic matter. Measurements of DIC ¹⁴C will be reported elsewhere, along with ³⁶Cl data. Nevertheless, the results show that dissolved carbon is modern down to the bottom, indicating the absence of carbon flux from volcanic emanation. DIC and p_{CO2} increase progressively with depth, suggesting that remineralization occurs through the water column, and may contribute significantly to the progressive increase in conductivity. The observed differences between the lakes, as well as contribution of other processes

such as the iron redox cycle or diagenetic flux from the bottom, will definitely need further investigation.

These results also confirm previous studies (Issa, Ohba, et al., 2014) that these lakes do not present a danger of catastrophic degassing through limnic eruption (Kling, 1988; Kling et al., 1987; Sigurdsson et al., 1987), since the deep p_{CO2} remains several orders of magnitude lower than saturation.

Mg^{2+} and Ca^{2+} are the dominant cations, representing up to 70%–80% of the cations sum (Table 2). Ca/Na (1.7–5.9) and Mg/Ca (0.9–1.4) are in a range of values typical of rivers from volcanic regions (Dessert et al., 2003; Louvat & Allègre, 1997). The Sr isotope ratio confirms this basaltic source of the dissolved load, with values from 0.7042 to 0.7059 similar to those determined by Marzoli et al. (1999) in trachytes from the Adamawa, and in good agreement with the result reported for Lake Nyos by Fantong et al. (2019). Each lake shows an ⁸⁷Sr/⁸⁶Sr ratio constant with depth and distinct from the others (Table 2). These variations may reflect either real heterogeneities within the volcanic source from one site to the next, or a slight contribution from weathering of the granitic basement variable from one lake to the next, depending on the local configuration of the contact between the granite basement and the volcanic cover and the path of water percolation.

The chloride concentrations range from 9 to 35 μeq/L (Table 2), amounting to only about 1% of the anions sum. By contrast with the increasing trends towards the bottom noted for the E.C., the Cl⁻ profiles are constant with depth below the thermocline (Figure 3). We
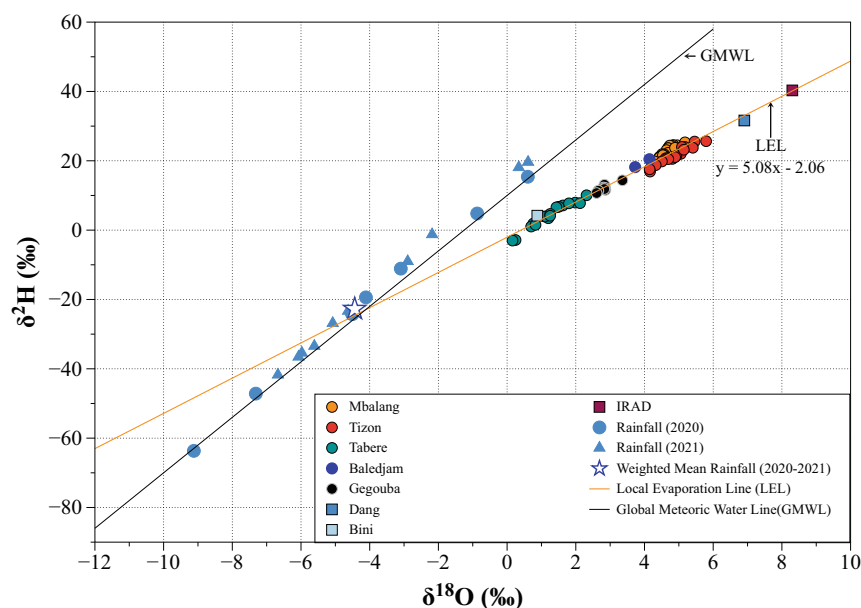
FIGURE 4 δ^2H versus δ^{18}O diagram.

also observe a very clear seasonal variation in the surface water of the three lakes that were monitored regularly, with maximum concentrations of chloride in April and May, that is, at the end of the dry season (Figure SI-5). Nevertheless, the amplitude of these variations remains limited (13% Mbalang, 20% Tabere, 16% Tizon). Each lake is therefore clearly characterized by a distinct mean concentration of chloride, increasing in order from Gegouba, Baledjam, Tabere and Mbalang, and up to Tizon Lake.

The chloride concentrations that we measured in our 18 rainwater samples range from 1.9 to 9.5 µeq/L, with a volume weighted mean of 4.0 ± 1.4 (1sd) µeq/L (Table 3). This value is within the range reported in the few previous studies discussing tropical rainfall (Freydier et al., 1998). The different lakes thus have 2.5–10 times more Cl$^-$ than does the rain, a critical parameter in the forthcoming discussion. The concentrations of Na$^+$ and Cl$^-$ in rainwater are well correlated with a slope of 0.97, indicating the marine origin of chloride in the rain. The relatively low concentration of Cl$^-$ in the lakes therefore implies that the rain contribution to the dissolved load of the lakes is very low, that is, from 3% to 14% for Na, and as little as 0.02%–0.06% for Ca, based on the classical correction assuming sea water element/Cl ratios in the rain (e.g., Negrel et al., 1993).

4.3 | O and H stable isotopes

The δ^2H versus δ^{18}O plot is shown in Figure 4. The rain data all plot within the margin of error on the GMWL line, with δ^{18}O values from −9.2‰ to 0.7‰. The isotopic ratios become increasingly depleted as the rainy season advances (Figure SI-6).

This depletion pattern was also shown by Tremoy et al. (2012) for rain samples from Niamey during the first part of the 2010 summer monsoon season and was interpreted as relating to the 'amount effect' (Dansgaard, 1964) resulting from increasing convective activity at the regional scale during the monsoon months.

The volume weighted mean composition of the rainfall is −4.44‰ ± 0.02‰ δ^{18}O and −22.76‰ ± 0.08‰ δ^2H (Table 3). It can be noted that this average is 1.5 ‰ more enriched than the estimate given by the RCWIP2 isoscapes model by Terzer-Wassmuth et al. (2021), most likely due to the wide spacing of GNIP stations in the region (closest stations in Garoua, Ndjamena and Yaounde, each of which is in a quite different hydroclimatic context).

The compositions of the lakes range from 0‰ to 8.5‰ δ^{18}O and from −3‰ to 40.5‰ δ^2H. In a very classic pattern, the data form a well-defined local evaporation line (LEL) with a slope of 5.08 ± 0.08 (RMSE = 1.12). The intersection of the LEL with the GMWL (−4.13‰ ± 0.16‰ δ^{18}O and −23.04‰ ± 0.80‰ δ^2H) is identical within error to the weighted mean rainfall composition. The smaller lakes IRAD and Dang have a more enriched composition than the deep lakes, as is to be expected for shallow reservoirs more affected by evaporation. By contrast, Bini lies among the depleted values of the other lakes, probably reflecting composition of the phreatic aquifer beneath the lake.

As for [Cl$^-$], the isotopic composition shows a clear seasonal variation in the surface waters, with a progressive depletion of δ^{18}O and δ^2H during the wet season, and parallel in the three lakes that we monitored (Figure SI-6). The amplitude of this variation is much smaller than for the rain, that is, 0.7‰, 1.6‰ and 3‰ for Mbalang, Tizon and Tabere respectively, compared to 10‰ for the rain. A similar seasonal stratification of the isotopic profile is also familiar in lakes under Mediterranean (e.g., Dean et al., 2015) or temperate climates (e.g., Assayag et al., 2008).

By comparison, much less variation is observed in the deep-water profiles, with each lake bearing a distinct composition (Figure 3). Mbalang and Tizon are the most enriched and both have δ^{18}O values close to 5‰, and Tabere and Gegouba are more depleted with values of 1.4 and 2.7. Baledjam, with only two samples from March 2019 analysed so far, appears intermediate between these two groups, although some seasonal variation cannot be ruled out in this shallow lake (13 m maximum depth).

FIGURE 5 $\delta^{18}O$ versus $[Cl^-]$ diagram with model solution curves of the water budget. (a) Evaporation alone. Small circles are the data. Large circles show the average values used in the calculations. (b) Model including the contribution from the watershed. Dashed lines are solutions with E/P variable, and solid lines are solutions with T/P variable. These solutions are unique when parameter $n.\theta$ is fixed.
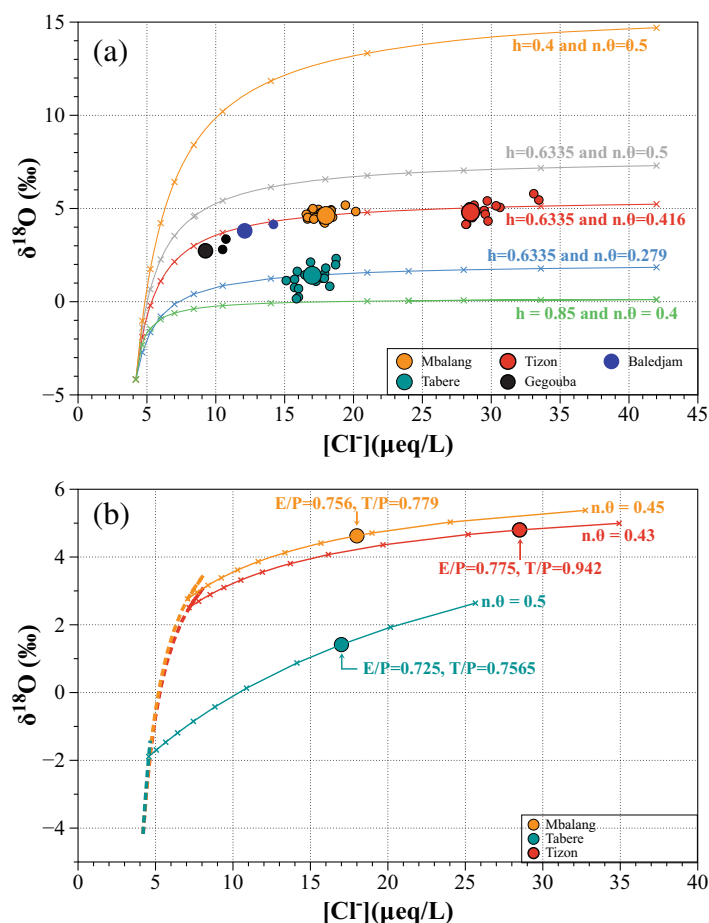
4.4 | $\delta^{18}O$ versus $[Cl^-]$ and hydrological budget

The results of different attempts to model the hydrological budget of the lakes are best illustrated in the $\delta^{18}O$ versus $[Cl^-]$ plot (Figure 5) to explain why they show different compositions for these conservative tracers, despite being located a priori under similar local climatic conditions. In Figure 5, the lakes are indeed discriminated even more clearly than in the isotope plot (Figure 4). In particular, Tizon is clearly distinguished from Mbalang by its chloride content, while they are similar in isotopic composition. Tabere, intermediate in chloride content, lies clearly below the others in isotopes.

The different model results obtained in our simulation scenarios are listed in Table 4.

As seen in Figure 5a, the standard model ($n.\theta = 0.5$) corresponding to the annual average humidity ($h = 0.6335$) does not allow to fit the observed values for any of the lakes (grey crosses). E/P values are thus different when calculated from $[Cl^-]$ and $\delta^{18}O$ (e.g., 0.766 and 0.506 for Mbalang, 0.753 and 0.244 for Tabere, etc.). Attributing this discrepancy to an underestimation of C_P would require that chloride concentration in the rain be as high as 7–14 meq/L, which seems very unlikely in the present state of data. The value of $n.\theta$ would need to be as low as 0.279 to account for the composition of Tabere, with $E/P = 0.753$ (blue crosses in Figure 5a). Similarly, Gegouba, Mbalang

and Tizon can be fitted by model curves with $n.\theta$ values ranging from 0.406 to 0.416 (red crosses in Figure 5a).

Alternatively, the compositions of all five lakes can be fitted with the model involving the watershed (Equations (5), (6) and (7)). Examples of solutions are illustrated in Figure 5b with cases where $n.\theta = 0.43$ for Tizon and 0.45 for Mbalang. The corresponding values of E/P and T/P are then (0.775, 0.942) for Tizon, and (0.756, 0.779) for Mbalang.

A significant outcome of this model is that the distinct position of Tabere can be simulated more easily, without calling for very low values of $n.\theta$ ($n.\theta = 0.5$, $E/P = 0.725$ and $T/P = 0.7565$ in the chosen example), clearly illustrating the influence of its larger watershed compared to the other lakes.

However, it is important to emphasize that these solutions are not unique, as has already been pointed out above. The solution of the system of Equations (6) and (7) varies between two limits, when either E/P or T/P tends towards 1, which also sets the upper and lower bounds for $n.\theta$. The example of Mbalang is illustrated in Figure SI-7. The lowest value of $n.\theta$ is 0.432 ($E/P = 0.9999$; $T/P = 0.499$). The highest value is 0.475 ($E/P = 0.563$; $T/P = 1$). The range of possible values for $n.\theta$ is thus very narrow, although still lower than the 'standard' value of 0.5.

The influence of the infiltration on the watershed (INF/P) is then shown in Figure 6, using the case of Tabere as an example.

TABLE 4 Model parameters and results of different simulation scenarios.

Evaporation alone on the lake with $n.\theta = 0.5$

$n.\theta$	δ_A	ε^*	ε_K	ε_T	E/P	T/P	INF/P	[Cl⁻]	δ_L	Lake
0.5	−8.74	9.6	5.2318	14.8318	0.766	-	-	17.95		Mbalang
					0.506	-	-		4.62	
0.5	−8.74	9.6	5.2318	14.8318	0.753	-	-	17		Tabere
					0.244	-	-		1.42	
0.5	−8.74	9.6	5.2318	14.8318	0.853	-	-	28.4		Tizon
					0.526	-	-		4.8	

Evaporation alone on the lake with $n.\theta$ variable

$n.\theta$	δ_A	ε^*	ε_K	ε_T	E/P	T/P	INF/P	[Cl⁻]	δ_L	Lake
0.416	−10.75	9.6	4.3528	-	0.766	-	-	17.949	4.628	Mbalang
0.279	−14.05	9.6	2.9193	-	0.753	-	-	17.004	1.4176	Tabere
0.406	−11	9.6	4.2482	-	0.8525	-	-	28.475	4.783	Tizon

Example of solutions with watershed model

$n.\theta$	δ_A	ε^*	ε_K	ε_T	E/P	T/P	INF/P	[Cl⁻]	δ_L	Lake
0.45	−9.94	9.6	4.7086	-	0.756	0.779	-	17.989	4.628	Mbalang
0.5	−8.74	9.6	5.2318	-	0.725	0.7565	-	17	1.419	Tabere
0.43	−10.42	9.6	4.4993	-	0.775	0.942	-	28.524	4.8	Tizon

Limits of solutions with watershed model for Mbalang

$n.\theta$	δ_A	ε^*	ε_K	ε_T	E/P	T/P	INF/P	[Cl⁻]	δ_L	Lake
0.4324	−10.36	9.6	4.5244	-	0.9999	0.499	-	18.001	4.6245	Mbalang ($n.\theta$ min)
0.475	−9.34	9.6	4.9702	-	0.563	1	-	17.985	4.622	Mbalang ($n.\theta$ max)

Evaporation alone on the lake with $n.\theta = 0.5$ and h variable

| $n.\theta$	δ_A	ε^*	ε_K	h
0.5	0.73	9.6	8.565	0.4
0.4	−5.51	9.6	6.852	0.4
0.3	−11.74	9.6	5.139	0.4
0.5	−11.25	9.6	3.56875	0.75
0.5	−12.86	9.6	2.1412	0.85
0.75	−11.03	9.6	3.2118	0.85
1	−9.2	9.6	4.2825	0.85
0.5	−4.41	9.6	7.1375	0.5
0.4	−8.56	9.6	5.71	0.5
0.3	−12.72	9.6	4.2825	0.5
0.25	−14.8	9.6	3.56875	0.5

Equation (7) shows that δ_L is fixed for a given value of $(T + \text{INF})/P$, while C_L decreases when INF/P increases (Equation (6)). In the example illustrated in the figure, a solution is obtained for E/P = 0.6, $(T + \text{INF})/P = 0.82$, and INF/P = 0.046. This solution is, once again not unique, with a set of possibilities with decreasing E/P and increasing $(T + \text{INF})/P$. However, the range of possible values is limited for INF/P, which reaches a maximum at 0.088, for E/P = 0.40 and $(T + \text{INF})/P = 0.92$.

5 | DISCUSSION

5.1 | Reconciling stable isotope and chloride mass balances

Because water stable isotopes and chloride are both tracers of evaporation process, they are supposed to provide similar estimates of this flux in lake systems where evaporation is a dominant factor of the

FIGURE 6 Two examples of solutions for the contribution of infiltration on the watershed. The isotopic composition of Tabere (green circle) can be fitted with $E/P = 0.725$, $T/P = 0.76$ and no contribution from the watershed (green line), or with $E/P = 0.60$, $T/P = 0.82$ and $INF/P = 0.046$ (blue line). The system of equations is undetermined, with an upper limit of INF/P of about 9%.
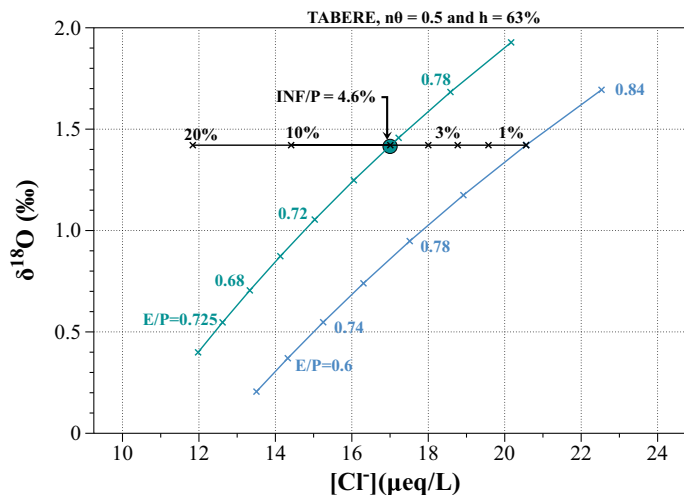
water budget. However, in this study, the E/P ratio calculated from ^{18}O and chloride mass balances are significantly different for all the five lakes studied here. The $n.\theta$ parameter of the Craig and Gordon model appears as critical to explain this discrepancy.

In the one-box model, the $n.\theta$ parameter can be tuned and by adopting smaller values than the commonly used $n.\theta$ parameter ($n.\theta = 0.5$), it is possible to reconcile both approaches. These results are thus fully coherent with the conclusion of Kebede et al. (2009), who showed that the results of the isotope mass balance model could not be reconciled with the observed slope of LEL for a set of 16 Ethiopian lakes of various sizes, unless they used a value of 0.5 for the θ parameter of Craig and Gordon's equation, instead of 1. Kebede et al. (2009) extended to small lakes the interpretation initially proposed by Gat (1995), that low values of θ reflect humidity buildup over a wide evaporating water surface. Specifically, these authors draw attention to lakes located in steep valleys or crater lakes with restricted ventilation over the lake, in which cases high rates of vapour recycling may occur.

Alternatively, the same constraint on the $n.\theta$ parameter is required for lakes Mbalang and Tizon, whereas another water supply term to the lake must be considered in the case of Lake Tabere, which drains the larger watershed. Lower values of $n.\theta$ in both cases (water supply by rainfall only and water input from the watershed in addition to rainfall) in Lakes Mbalang and Tizon would suggest that the standard value of 0.5 may not accurately represent the processes that occur in certain tropical systems.

Our various attempts in combining ^{18}O and chloride to obtain the same water mass budget highlight the sensitivity of the hydro-isotopic balance calculation to the choice of parameters and allow the estimation of other terms of the water budget.

5.2 | Sensitivity of the isotope mass balance to Craig and Gordon's model parameters

The different tests described above shed light on the extreme sensitivity of Craig and Gordon's model to the choice of parameters, and

underline the non-uniqueness of the solutions. This caveat must thus be kept in mind when trying to obtain quantitative information about the lakes' water budgets. In addition, the hypotheses of steady state and homogeneity can also only be considered as a first order approximations devoted to sensitivity testing. For instance, the strong influence of h on the results is illustrated in Figure SI-3, where it can be seen that values of h lower than the annual average (i.e., $h = 0.4$ is the annual average of monthly minima) shift the model curves towards higher δ^{18}O and thus increase the discrepancy between δ^{18}O and [Cl$^-$]. However, the precise determination of a more representative average value of humidity to be used in a steady state simulation would require a detailed analysis of the relationship between humidity and evaporation flux, which is beyond the scope of the present study.

Once a given value is selected for h, the next main parameter with a strong influence on the model results is δ_A. We illustrate in Figure SI-3 and Figure SI-8 the relationship between δ_A and $n.\theta$ for a set of various solutions satisfying the observed slope of 5.08 for the LEL, provided that the atmospheric composition lies on the GMWL. Except for the lowest and unlikely values of $n.\theta$, these model values of δ_A are enriched with respect to the composition at equilibrium with the average precipitation (-13.8‰). While this situation is comparable with the model results obtained by Vallet-Coulomb et al. (2008) for Lake Ihotry in Madagascar, it is contrary to the direct measurement in vapour phase obtained by Tremoy et al. (2012) who used laser mass spectrometry around Niamey. Such vapour measurement will thus be needed, both to elucidate the rain-vapour relationship in the regional climate conditions of the study area, and then to restrict drastically the range of possible solutions to the model budget.

Moreover, it must be kept in mind that the results of our model are based on the simplifying assumption that the isotopic composition of the water vapour over the lakes lies on the GMWL in the isotope plot. This assumption allows us to obtain a unique solution to the system of equations linking chloride and isotopes budgets. However, a noticeable shortcoming of this assumption is that it neglects the effect of the mixing of vapour evaporated from the lake with the synoptic atmospheric vapour, whereas the precise consequence of this

recycling process is that the resulting atmospheric composition is displaced out of the GMWL. Therefore, it must be emphasized once again that the procedure described here is useful only to evaluate the range of uncertainty associated with water budget estimation. The impact of recycling on the model could be simulated by using the same procedure with arbitrary values selected a priori for δ_A and for the mixing proportion between evaporation from the lake and synoptic atmosphere. However, this again renders the system of equations undetermined.

5.3 | Assessment of the different terms of the water budget

In addition to the evaporation term for which conservative tracers are good indicators, our attempt to reconcile the isotopic and chemical balances allowed to estimate other water balance terms. Indeed, our simulations show that the water inflow from the watershed, either as surface runoff or subsurface flow, can also make a significant contribution to the water budget of a lake. Despite the non-determination of the system of equations in this case too, the range of possible influence of this input can be evaluated.

In the case of Tabere in the example above, the inflow from the watershed may be as high as 40% of the rain on the lake itself. The results also show that taking this input into account allows to reconcile isotope and chloride mass balances, provided that transpiration dominates evaporation on the watershed. Moreover, it is of note that this model implies that transpiration from the watershed must be on the same order of magnitude as evaporation from the lake if it is to fit the observations (i.e., $T/P \approx E/P$). Although still speculative at this stage owing to the large range of uncertainties discussed above, this conclusion is in line with the on-going debate about global comparative estimates of transpiration versus evaporation (e.g., Jasechko et al., 2013 and references therein). Further testing of this hypothesis will require sampling and analyses of water flowing on the surface and percolating underground in the watershed.

6 | CONCLUSION

We provide here an initial comprehensive data set on the hydrology and geochemistry of the volcanic Adamawa lakes, which we find have the common characteristics of monomictic maar lakes. Our results show distinct signatures in $\delta^{18}O$, δ^2H, chloride and electrical conductivity across the five lakes. Despite their relative proximity—and thus similar rainfall input—these lakes constitute a valuable benchmark for testing our ability to model the hydrological budget based on these two conservative geochemical tracers.

Our simulation results show that the standard version of Craig and Gordon's equation gives inconsistent results when used to compare stable isotopes with chloride budgets. More precisely, values lower than those usually accepted are required for the physical parameters (so-called '$n.\theta$' factor less than 0.5) to reconcile the two

tracers. This conclusion is in agreement with the results of Kebede et al. (2009) for Ethiopian lakes, and confirms that it is a common feature for tropical lakes of both arid and humid regions.

We also show that accounting for upstream watershed contributions through runoff and subsurface flow offers a useful alternative to close the water budget. Importantly, we found that the specific fluxes of transpiration from the watershed and of evaporation from the lake must be on the same order of magnitude, or slightly in favour of transpiration, to fit the observations. Despite the large range of uncertainty of the model output, the water budget of the lakes was always dominated by evaporation over outflow (50% < E/I < 90%).

Another outcome of this study is the confirmation of previous studies showing that direct isotopic measurements of atmospheric moisture are required to discriminate between the different models and reduce the range of possible solutions. Sampling and analyses of surface and sub-surface water flowing into lakes will also be required to decipher the exact contribution of watershed inflows to the hydrological budget of lakes.

DATA AVAILABILITY STATEMENT
The data that support the findings of this study are available in the submitted manuscript.

ORCID
Souleyman Abba 🔟 https://orcid.org/0000-0002-3233-2013

REFERENCES
Adallal, R., Vallet-Coulomb, C., Vidal, L., Benkaddour, A., Rhoujjati, A., & Sonzogni, C. (2019). Modelling lake water and isotope mass balance variations of Lake Azigza in the Moroccan Middle Atlas under Mediterranean climate. *Regional Environmental Change, 19*(8), 2697–2709. https://doi.org/10.1007/s10113-019-01566-9

Adrian, R., O'Reilly, C. M., Zagarese, H., Baines, S. B., Hessen, D. O., Keller, W., Livingstone, D. M., Sommaruga, R., Straile, D., Van Donk, E., Weyhenmeyer, G. A., & Winder, M. (2009). Lakes as sentinels of climate change. *Limnology and Oceanography, 54*(6part2), 2283–2297. https://doi.org/10.4319/lo.2009.54.6_part_2.2283

Araguäs-Araguäs, L., Froehlich, K., & Rozanski, K. (2000). Deuterium and oxygen-18 isotope composition of precipitation and atmospheric moisture. *Hydrological Processes, 14*(8), 1341–1355. https://doi.org/10.1002/1099-1085(20000615)14:8<1341::AID-HYP983>3.0.CO;2-Z

Assayag, N., Jézéquel, D., Ader, M., Viollier, E., Michard, G., Prévot, F., & Agrinier, P. (2008). Hydrological budget, carbon sources and biogeochemical processes in Lac Pavin (France): Constraints from δ18O of

water and δ13C of dissolved inorganic carbon. *Applied Geochemistry*, *23*(10), 2800–2816. https://doi.org/10.1016/j.apgeochem.2008.04.015

Awaleh, M. O., Hoch, F. B., Boschetti, T., Soubaneh, Y. D., Egueh, N. M., Elmi, S. A., Mohamed, J., & Khaireh, M. A. (2015). The geothermal resources of the Republic of Djibouti—II: Geochemical study of the Lake Abhe geothermal field. *Journal of Geochemical Exploration*, *159*, 129–147. https://doi.org/10.1016/j.gexplo.2015.08.011

Bader, J.-C., Lemoalle, J., & Leblanc, M. (2011). Modèle hydrologique du Lac Tchad. *Hydrological Sciences Journal*, *56*(3), 411–425. https://doi.org/10.1080/02626667.2011.560853

Bergonzini, L., Gibert, É., Winckel, A., & Merdaci, O. (2001). Bilans hydrologique et isotopiques (18O et 2H) du lac Massoko, Tanzanie. Quantification des échanges lac–eaux souterraines. *Comptes Rendus de l'Académie des Sciences*, *333*(10), 617–623. https://doi.org/10.1016/S1251-8050(01)01672-X

Bouchez, C., Goncalves, J., Deschamps, P., Vallet-Coulomb, C., Hamelin, B., Doumnang, J.-C., & Sylvestre, F. (2016). Hydrological, chemical, and isotopic budgets of Lake Chad: A quantitative assessment of evaporation, transpiration and infiltration fluxes. *Hydrology and Earth System Sciences*, *20*(4), 1599–1619. https://doi.org/10.5194/hess-20-1599-2016

Bouchez, C., Pupier, J., Benedetti, L., Deschamps, P., Guillou, V., Keddadouche, K., Aumaître, G., Arnold, M., & Bourlès, D. (2015). Isotope dilution-AMS technique for 36 Cl and Cl determination in low chlorine content waters. *Chemical Geology*, *404*, 62–70. https://doi.org/10.1016/j.chemgeo.2015.03.022

Branchu, P., & Bergonzini, L. (2004). Chloride concentrations in Lake Tanganyika: An indicator of the hydrological budget? *Hydrology and Earth System Sciences*, *8*(2), 256–265. https://doi.org/10.5194/hess-8-256-2004

Butcher, J. B., Nover, D., Johnson, T. E., & Clark, C. M. (2015). Sensitivity of lake thermal and mixing dynamics to climate change. *Climatic Change*, *129*(1–2), 295–305. https://doi.org/10.1007/s10584-015-1326-1

Calvi, C., Dapeña, C., Quiroz Londoño, O. M., & Martinez, D. E. (2022). Assessing recharge process in plain catchments using isotopic and hydrochemical techniques. *Groundwater for Sustainable Development*, *19*, 100828. https://doi.org/10.1016/j.gsd.2022.100828

Cole, J. J., Caraco, N. F., Kling, G. W., & Kratz, T. K. (1994). Carbon dioxide supersaturation in the surface waters of lakes. *Science*, *265*(5178), 1568–1570. https://doi.org/10.1126/science.265.5178.1568

Craig, H., & Gordon, L. I. (1965). Deuterium and oxygen 18 variations in the ocean and the marine atmosphere. Stable Isotopes in Oceanographic Studies and Paleotemperatures. In E. Tongiorgi, V. Lischi, & Figli (Eds.), *Proceedings of the Third Spoleto Conference Spoleto, Italy*.

Crosbie, R. S., Peeters, L. J. M., Herron, N., McVicar, T. R., & Herr, A. (2018). Estimating groundwater recharge and its associated uncertainty: Use of regression kriging and the chloride mass balance method. *Journal of Hydrology*, *561*, 1063–1080. https://doi.org/10.1016/j.jhydrol.2017.08.003

Dansgaard, W. (1964). Stable isotopes in precipitation. *Tellus*, *16*(4), 436–468. https://doi.org/10.3402/tellusa.v16i4.8993

De Crop, W., & Verschuren, D. (2019). Determining patterns of stratification and mixing in tropical crater lakes through intermittent water-column profiling: A case study in western Uganda. *Journal of African Earth Sciences*, *153*, 17–30. https://doi.org/10.1016/j.jafrearsci.2019.02.019

De Crop, W., & Verschuren, D. (2021). Mixing regimes in the equatorial crater lakes of western Uganda. *Limnologica*, *90*, 125891. https://doi.org/10.1016/j.limno.2021.125891

Dean, J. R., Eastwood, W. J., Roberts, N., Jones, M. D., Yiğitbaşıoğlu, H., Allcock, S. L., Woodbridge, J., Metcalfe, S. E., & Leng, M. J. (2015). Tracking the hydro-climatic signal from lake to sediment: A field study

from central Turkey. *Journal of Hydrology*, *529*, 608–621. https://doi.org/10.1016/j.jhydrol.2014.11.004

Delalande, M., Bergonzini, L., Beal, F., Garcin, Y., Majule, A., & Williamson, D. (2005). Contribution to the detection of Lake Masoko (Tanzania) groundwater outflow: Isotopic evidence (18O, D)/Contribution à la détection des pertes souterraines du Lac Masoko (Tanzanie): Évidences isotopiques (18O, D). *Hydrological Sciences Journal*, *50*(5), 10. https://doi.org/10.1623/hysj.2005.50.5.867

Delalande, M., Bergonzini, L., Branchu, P., Filly, A., & Williamson, D. (2008). Hydroclimatic and geothermal controls on the salinity of Mbaka Lakes (SW Tanzania): Limnological and paleolimnological implications. *Journal of Hydrology*, *359*(3–4), 274–286. https://doi.org/10.1016/j.jhydrol.2008.07.007

Delalande, M., Bergonzini, L., & Massault, M. (2008). Mbaka lakes isotopic (18O and 2H) and water balances: Discussion on the used atmospheric moisture compositions. *Isotopes in Environmental and Health Studies*, *44*(1), 71–82. https://doi.org/10.1080/10256010801887414

Delalande-Le Mouëllic, M., Gherardi, F., Williamson, D., Kajula, S., Kraml, M., Noret, A., Abdallah, I., Mwandapile, E., Massault, M., Majule, A., & Bergonzini, L. (2015). Hydrogeochemical features of Lake Ngozi (SW Tanzania). *Journal of African Earth Sciences*, *103*, 153–167. https://doi.org/10.1016/j.jafrearsci.2014.11.004

Dessert, C., Dupré, B., Gaillardet, J., François, L. M., & Allègre, C. J. (2003). Basalt weathering laws and the impact of basalt weathering on the global carbon cycle. *Chemical Geology*, *202*(3–4), 257–273. https://doi.org/10.1016/j.chemgeo.2002.10.001

Dinçer, T., Hutton, L. G., & Kupee, B. B. J. (1979). Study, using stable isotopes, of surface-groundwater relations and evapo-transpiration in the Okavonga swamp, Botswana. *Isotope Hydrology*, *1*, 3–26.

Dogramaci, S., Firmani, G., Hedley, P., Skrzypek, G., & Grierson, P. F. (2015). Evaluating recharge to an ephemeral dryland stream using a hydraulic model and water, chloride and isotope mass balance. *Journal of Hydrology*, *521*, 520–532. https://doi.org/10.1016/j.jhydrol.2014.12.017

Fantong, W. Y., Kamtchueng, B. T., Ishizaki, Y., Fru, E. C., Fantong, E. B., Wirmvem, M. J., Aka, F. T., Nlend, B., Harman, D., Ueda, A., Kusakabe, M., Tanyileke, G., & Ohba, T. (2019). Major ions, δ18O, δ13C and 87Sr/86Sr compositions of water and precipitates from springs along the Cameroon volcanic line (Cameroon, west Africa): Implications for provenance and volcanic hazards. *Journal of African Earth Sciences*, *150*, 12–22. https://doi.org/10.1016/j.jafrearsci.2018.09.025

Freydier, R., Dupre, B., & Lacaux, J. P. (1998). Precipitation chemistry in intertropical Africa. *Atmospheric Environment*, *32*(4), 749–765. https://doi.org/10.1016/S1352-2310(97)00342-7

Garcin, Y., Deschamps, P., Ménot, G., de Saulieu, G., Schefuß, E., Sebag, D., Dupont, L. M., Oslisly, R., Brademann, B., Mbusnum, K. G., Onana, J.-M., Ako, A. A., Epp, L. S., Tjallingii, R., Strecker, M. R., Brauer, A., & Sachse, D. (2018). Early anthropogenic impact on Western Central African rainforests 2, 600 y ago. *Proceedings of the National Academy of Sciences*, *115*(13), 3261–3266. https://doi.org/10.1073/pnas.1715336115

Gat, J. R. (1995). Stable isotopes in fresh and saline lakes. In A. Lerman, D. Imboden, & J. Gat (Eds.), *Physics and chemistry of lakes* (pp. 139–166). Springer-Verlag.

Gat, J. R. (2010). *Isotope hydrology: A study of the water cycle*. Imperial College Press.

Gat, J. R., Bowser, C. J., & Kendall, C. (1994). The contribution of evaporation from the Great Lakes to the continental atmosphere: Estimate based on stable isotope data. *Geophysical Research Letters*, *21*(7), 557–560. https://doi.org/10.1029/94GL00069

Gat, J. R., Shemesh, A., Tziperman, E., Hecht, A., Georgopoulos, D., & Basturk, O. (1996). The stable isotope composition of waters of the eastern Mediterranean Sea. *Journal of Geophysical Research: Oceans*, *101*(C3), 6441–6451. https://doi.org/10.1029/95JC02829

Gèze, B. (1943). *Géographie physique et géologie du Cameroun occidental (Editions du Muséum)*. Muséum National d'Histoire Naturelle.

Gibson, J. J., Birks, S. J., & Yi, Y. (2016). Stable isotope mass balance of lakes: A contemporary perspective. *Quaternary Science Reviews*, 131, 316–328. https://doi.org/10.1016/j.quascirev.2015.04.013

Gibson, J. J., & Edwards, T. W. D. (2002). Regional water balance trends and evaporation-transpiration partitioning from a stable isotope survey of lakes in northern Canada: Regional water balance using stable isotopes. *Global Biogeochemical Cycles*, 16(2), 1–14. https://doi.org/10.1029/2001GB001839

Gonfiantini, R. (1986). Environmental isotopes in lake studies. In *Handbook of environmental isotope geochemistry* (Vol. 3, pp. 113–168). Elsevier.

Gurrieri, J. T., & Furniss, G. (2004). Estimation of groundwater exchange in alpine lakes using non-steady mass-balance methods. *Journal of Hydrology*, 297(1–4), 187–208. https://doi.org/10.1016/j.jhydrol.2004.04.021

Horita, J., & Wesolowski, D. J. (1994). Liquid-vapor fractionation of oxygen and hydrogen isotopes of water from the freezing to the critical temperature. *Geochimica et Cosmochimica Acta*, 58(16), 3425–3437. https://doi.org/10.1016/0016-7037(94)90096-5

Issa, Aka Tongwa, F., Mouliom, A. G., Rouwet, D., Fantong, W. Y., Chako Tchamabé, B., Ohba, T., Yoshida, Y., Sighomnou, D., Sigha, N., & Kusakabe, M. (2014). $\delta^{18}O$ and δD variations in some volcanic lakes on the Cameroon Volcanic Line (West-Africa): Generating isotopic baseline data for volcano monitoring and surveillance in Cameroon. *Journal of Limnology*, 74, 95–113. https://doi.org/10.4081/jlimnol.2014.966

Issa, Ohba, T., Chako Tchamabé, B., Padrón, E., Hernández, P., Eneke Takem, E. G., Barrancos, J., Sighomnoun, D., Ooki, S., Nkamdjou, S., Kusakabe, M., Yoshida, Y., & Dionis, S. (2014). Gas emission from diffuse degassing structures (DDS) of the Cameroon volcanic line (CVL): Implications for the prevention of CO_2-related hazards. *Journal of Volcanology and Geothermal Research*, 283, 82–93. https://doi.org/10.1016/j.jvolgeores.2014.07.001

Jasechko, S., Sharp, Z. D., Gibson, J. J., Birks, S. J., Yi, Y., & Fawcett, P. J. (2013). Terrestrial water fluxes dominated by transpiration. *Nature*, 496(7445), 347–350. https://doi.org/10.1038/nature11983

Kebede, S., Lamb, H., Telford, R., Leng, M., & Umer, M. (2002). Lake—Groundwater relationships, oxygen isotope balance and climate sensitivity of the Bishoftu Crater Lakes, Ethiopia. In E. O. Odada & D. O. Olago (Eds.), *The east African Great Lakes: Limnology, palaeolimnology and biodiversity* (Vol. 12, pp. 261–275). Springer. https://doi.org/10.1007/0-306-48201-0_9

Kebede, S., Travi, Y., & Rozanski, K. (2009). The $\delta^{18}O$, δ^2H enrichment of Ethiopian lakes. *Journal of Hydrology*, 365(3–4), 173–182. https://doi.org/10.1016/j.jhydrol.2008.11.027

Kirchner, J. W., Tetzlaff, D., & Soulsby, C. (2010). Comparing chloride and water isotopes as hydrological tracers in two Scottish catchments. *Hydrological Processes*, 24(12), 1631–1645. https://doi.org/10.1002/hyp.7676

Kling, G. W. (1988). Comparative transparency, depth of mixing, and stability of stratification in lakes of Cameroon, West Africa 1: Lake mixing in Cameroon. *Limnology and Oceanography*, 33(1), 27–40. https://doi.org/10.4319/lo.1988.33.1.0027

Kling, G. W., Clark, M. A., Wagner, G. N., Compton, H. R., Humphrey, A. M., Devine, J. D., Evans, W. C., Lockwood, J. P., Tuttle, M. L., & Koenigsberg, E. J. (1987). The 1986 Lake Nyos gas disaster in Cameroon, West Africa. *Science*, 236(4798), 169–175. https://doi.org/10.1126/science.236.4798.169

Lerman, A., Imboden, D. M., & Gat, J. R. (1995). *Physics and chemistry of lakes*. Springer Berlin Heidelberg. https://doi.org/10.1007/978-3-642-85132-2

Louvat, P., & Allègre, C. J. (1997). Present denudation rates on the Island of Réunion determined by river geochemistry: Basalt weathering and mass budget between chemical and mechanical erosions. *Geochimica et Cosmochimica Acta*, 61(17), 3645–3669. https://doi.org/10.1016/S0016-7037(97)00180-4

Marzoli, A., Renne, P. R., Piccirillo, E. M., Francesca, C., Bellieni, G., Melfi, A. J., Nyobe, J. B., & N'ni, J. (1999). Silicic magmas from the continental Cameroon Volcanic Line (Oku, Bambouto and Ngaoundere): 40 Ar-39 Ar dates, petrology, Sr-Nd-O isotopes and their petrogenetic significance. *Contributions to Mineralogy and Petrology*, 135(2–3), 133–150. https://doi.org/10.1007/s004100050502

Masse-Dufresne, J., Barbecot, F., Baudron, P., & Gibson, J. (2021). Quantifying floodwater impacts on a lake water budget via volume-dependent transient stable isotope mass balance. *Hydrology and Earth System Sciences*, 25(6), 3731–3757. https://doi.org/10.5194/hess-25-3731-2021

Merlivat, L. (1978). Molecular diffusivities of H216O, HD16O, and H218O in gases. *The Journal of Chemical Physics*, 69(6), 2864. https://doi.org/10.1063/1.436884

Nachiappan, R. P., Kumar, B., & Manickavasagam, R. (2002). Estimation of subsurface components in the water balance of Lake Nainital (Kumaun Himalaya, India) using environmental isotopes. *Hydrological Sciences Journal*, 47(suppl 1), S41–S54. https://doi.org/10.1080/02626660209493021

Négrel, P., Allègre, C. J., Dupré, B., & Lewin, E. (1993). Erosion sources determined by inversion of major and trace element ratios and strontium isotopic ratios in river water: The Congo Basin case. *Earth and Planetary Science Letters*, 120(1–2), 59–76. https://doi.org/10.1016/0012-821X(93)90023-3

Ngos, S., & Giresse, P. (2012). The Holocene sedimentary and pyroclastic accumulations of two crater lakes (Mbalang, Tizong) of the volcanic plateau of Adamawa (Cameroon): Palaeoenvironmental reconstruction. *The Holocene*, 22(1), 31–42. https://doi.org/10.1177/0959683611409779

Nguetsop, V. F., Bentaleb, I., Favier, C., Martin, C., Bietrix, S., Giresse, P., Servant-Vildary, S., & Servant, M. (2011). Past environmental and climatic changes during the last 7200 cal yr BP in Adamawa plateau (Northern-Cameroun) based on fossil diatoms and sedimentary carbon isotopic records from Lake Mbalang. *Climate of the Past*, 7(4), 1371–1393. https://doi.org/10.5194/cp-7-1371-2011

Poulin, C., Hamelin, B., Vallet-Coulomb, C., Amngar, G., Loukman, B., Cretaux, J.-F., Doumnang, J.-C., Mahamat Nour, A., Menot, G., Sylvestre, F., & Deschamps, P. (2019). Unraveling the hydrological budget of isolated and seasonally contrasted subtropical lakes. *Hydrology and Earth System Sciences*, 23(3), 1705–1724. https://doi.org/10.5194/hess-23-1705-2019

Rippstein, G. (1986). *Étude sur la végétation de 1'Adamoua*. Maisons-Alfort.

Saleem, M., & Jeelani, G. (2017). Geochemical, isotopic and hydrological mass balance approaches to constrain the lake water–groundwater interaction in Dal Lake, Kashmir Valley. *Environmental Earth Sciences*, 76(15), 533. https://doi.org/10.1007/s12665-017-6865-5

Saulnier-Talbot, É., Gregory-Eaves, I., Simpson, K. G., Efitre, J., Nowlan, T. E., Taranu, Z. E., & Chapman, L. J. (2014). Small changes in climate can profoundly alter the dynamics and ecosystem services of tropical crater lakes. *PLoS One*, 9(1), e86561. https://doi.org/10.1371/journal.pone.0086561

Schaaff, V., Sebag, D., Makou, M., Grossi, V., Antheaume, I., Hamelin, B., Garcin, Y., Ngounou Ngatcha, B., Deschamps, P., & Ménot, G. (2023). Modeling the decomposition signal and correcting bulk organic data from a peat deposit, a case study at low latitudes (Cameroon). *Organic Geochemistry*, 179, 104589. https://doi.org/10.1016/j.orggeochem.2023.104589

Sigurdsson, H., Devine, J. D., Tchua, F. M., Presser, F. M., Pringle, M. K. W., & Evans, W. C. (1987). Origin of the lethal gas burst from Lake Monoun, Cameroun. *Journal of Volcanology and Geothermal Research*, 31(1–2), 1–16. https://doi.org/10.1016/0377-0273(87)90002-3

Suchel, J. B. (1988). *Les climats du Cameroun*. Université de Bordeaux.

Tanyileke, G., Ntchantcho, R., Fantong, W. Y., Aka, F. T., & Hell, J. V. (2019). 30 years of the lakes Nyos and Monoun gas disasters: A

scientific, technological, institutional and social adventure. *Journal of African Earth Sciences*, *150*, 415–424. https://doi.org/10.1016/j.jafrearsci.2018.11.022

Terzer-Wassmuth, S., Wassenaar, L. I., Welker, J. M., & Araguás-Araguás, L. J. (2021). Improved high-resolution global and regionalized iso-scapes of $\delta^{18}O$, δ^2H and D-excess in precipitation. *Hydrological Processes*, *35*(6). https://doi.org/10.1002/hyp.14254

Tremoy, G., Vimeux, F., Mayaki, S., Souley, I., Cattani, O., Risi, C., Favreau, G., & Oi, M. (2012). A 1-year long δ18O record of water vapor in Niamey (Niger) reveals insightful atmospheric processes at different timescales. *Geophysical Research Letters*, *39*(8), L08805. https://doi.org/10.1029/2012GL051298

Vallet-Coulomb, C., Gasse, F., & Sonzogni, C. (2008). Seasonal evolution of the isotopic composition of atmospheric water vapour above a tropical lake: Deuterium excess and implication for water recycling. *Geochimica et Cosmochimica Acta*, *72*(19), 4661–4674. https://doi.org/10.1016/j.gca.2008.06.025

Vallet-Coulomb, C., Legesse, D., Gasse, F., Travi, Y., & Chernet, T. (2001). Lake evaporation estimates in tropical Africa (Lake Ziway, Ethiopia). *Journal of Hydrology*, *245*(1–4), 1–18. https://doi.org/10.1016/S0022-1694(01)00341-9

Vincens, A., Buchet, G., Servant, M., & ECOFIT Mbalang Collaborators. (2010). Vegetation response to the "African humid period" termination in Central Cameroon (7° N)—New pollen insight from Lake Mbalang. *Climate of the Past*, *6*(3), 281–294. https://doi.org/10.5194/cp-6-281-2010

Wang, W., Lee, X., Xiao, W., Liu, S., Schultz, N., Wang, Y., Zhang, M., & Zhao, L. (2018). Global lake evaporation accelerated by changes in surface energy allocation in a warmer climate. *Nature Geoscience*, *11*(6), 410–414. https://doi.org/10.1038/s41561-018-0114-8

Wirrmann, D. (1994). *Les lacs Baledjam, Gagouba, Mbalang, Tabéré et Tizon, région de Ngaoundéré, province de l'Adamaoua*. ORSTOM.

Wolff, C., Kristen-Jenny, I., Schettler, G., Plessen, B., Meyer, H., Dulski, P., Naumann, R., Brauer, A., Verschuren, D., & Haug, G. H. (2014). Modern seasonality in Lake Challa (Kenya/Tanzania) and its sedimentary documentation in recent lake sediments. *Limnology and Oceanography*, *59*(5), 1621–1636. https://doi.org/10.4319/lo.2014.59.5.1621

Yakir, D., & Wang, X.-F. (1996). Fluxes of CO_2 and water between terrestrial vegetation and the atmosphere estimated from isotope measurements. *Nature*, *380*(6574), 515–517. https://doi.org/10.1038/380515a0

Yao, F., Livneh, B., Rajagopalan, B., Wang, J., Crétaux, J.-F., Wada, Y., & Berge-Nguyen, M. (2023). Satellites reveal widespread decline in global lake water storage. *Science*, *380*(6646), 743–749. https://doi.org/10.1126/science.abo2812

Yeghicheyan, D., Grinberg, P., Alleman, L. Y., Belhadj, M., Causse, L., Chmeleff, J., Cordier, L., Djouraev, I., Dumoulin, D., Dumont, J., Freydier, R., Mariot, H., Cloquet, C., Kumkrong, P., Malet, B., Jeandel, C., Marquet, A., Riotte, J., Tharaud, M., … Mester, Z. (2021). Collaborative determination of trace element mass fractions and isotope ratios in AQUA-1 drinking water certified reference material. *Analytical and Bioanalytical Chemistry*, *413*(20), 4959–4978. https://doi.org/10.1007/s00216-021-03456-8

SUPPORTING INFORMATION

Additional supporting information can be found online in the Supporting Information section at the end of this article.